PL-TR-94-2180

Deactivation of Vibrationally-Excited NO and CO_2 by O-Atoms

Harvey V. Lilenfeld

McDonnell Douglas Corporation
P.O. Box 516
St Louis, MO 63166-0516

June 1994

Final Report
28 September 1989-15 June 1994

APPROVED FOR PUBLIC RELEASE; DISTRIBUTION UNLIMITED

PHILLIPS LABORATORY
Directorate of Geophysics
AIR FORCE MATERIEL COMMAND
HANSCOM AFB, MA 01731-3010

"This technical report has been reviewed and is approved for publication."

DEAN F. KIMBALL
Contract Manager
Simulation Branch

WILLIAM A. M. BLUMBERG, Chief
Simulation Branch
Optical Environment Division

ROGER A. VAN TASSEL, Director
Optical Environment Division

This report has been reviewed by the ESC Public Affairs Office (PA) and is releasable to the National Technical Information Service (NTIS).

Qualified requestors may obtain additional copies from the Defense Technical Information Center (DTIC). All Others should apply to the National Technical Information Service (NTIS).

If your address has changed, if you wish to be removed from the mailing list, or if the addressee is no longer employed by your organization, please notify PL/IM, 29 Randolph Road, Hanscom AFB, MA 01731-3010. This will assist us in maintaining a current mailing list.

Do not return copies of this report unless contractual obligations or notices on a specific document require that it be returned.

REPORT DOCUMENTATION PAGE

Form Approved
OMB No. 0704-0188

1. AGENCY USE ONLY (Leave blank)	2. REPORT DATE	3. REPORT TYPE AND DATES COVERED
	June 1994	Final Technical 9/28/89-6/15/94

4. TITLE AND SUBTITLE

Deactivation of Vibrationally-Excited NO and CO_2 by O-Atoms

5. FUNDING NUMBERS

F19628-89-C-0191
PE 61102F
PR 2310
TA G4
WU CD

6. AUTHOR(S)

H. V. Lilenfeld

7. PERFORMING ORGANIZATION NAME(S) AND ADDRESS(ES)

McDonnell Douglas Aerospace
P.O. Box 516
St. Louis, MO 63166-0516

8. PERFORMING ORGANIZATION REPORT NUMBER

9. SPONSORING/MONITORING AGENCY NAME(S) AND ADDRESS(ES)

Phillips Laboratory
29 Randolph Road
Hanscom AFB, MA 01731-3010
Contract Manager: Dean Kimball/GPOS

10. SPONSORING/MONITORING AGENCY REPORT NUMBER

PL-TR-94-2180

11. SUPPLEMENTARY NOTES

12a. DISTRIBUTION/AVAILABILITY STATEMENT

Approved for public release; distribution unlimited

12b. DISTRIBUTION CODE

13. ABSTRACT *(Maximum 200 words)*

Two laboratory studies were performed to measure the rates of deactivation of vibrationally-excited species by atomic oxygen. In the first study an apparatus was constructed to measure the rate of deactivation of NO(v=1) by O. The apparatus consisted of a microwave generator to produce atomic oxygen, a fast flow reactor to deliver the atomic oxygen, a pulsed CO laser to excite NO and an EPR spectrometer to measure the atomic oxygen concentration. A rate constant, for the deactivation of NO(v=1) by O, $5\pm1\times10^{-11}$ $cm^3molecule^{-1}s^{-1}$ was measured in the temperature range 200-350K. In the second study, an apparatus consisting of a large diameter fast flow reactor with two microwave discharges (one to dissociate O_2 into oxygen atoms and a second to vibrationally excite CO_2), and a laser diode spectrometer to monitor the vibrationally-excited CO_2 was built. The room temperature rate constant for deactivation of CO_2 (01^10) by O was determined to be $5\pm2\times10^{-13}$ $cm^3molecule^{-1}s^{-1}$.

14. SUBJECT TERMS

upper-atmosphere kinetics, deactivation, vibrational relaxation, atomic oxygen, vibrationally-excited CO_2, vibrationally-excited NO

15. NUMBER OF PAGES

28

16. PRICE CODE

17. SECURITY CLASSIFICATION OF REPORT	18. SECURITY CLASSIFICATION OF THIS PAGE	19. SECURITY CLASSIFICATION OF ABSTRACT	20. LIMITATION OF ABSTRACT
Unclassified	Unclassified	Unclassified	SAR

Contents

1. Summary 1
2. Introduction 1
3. Measurement of the Deactivation of NO(v=1) 2
   3.1 Background 2
   3.2. Experiment 2
      3.2.1 Flow Measurements 3
      3.2.2 Production and Measurement of Atomic Oxygen. 3
      3.2.3 Excitation of NO(v=1) 4
      3.2.4 Temperature Regulation 5
      3.2.5 Data Collection and Analysis 5
   3.3 Results 5
      3.3.1 Operation of the CO Laser on the P(11)8→7 line 6
      3.3.2 Measurement of the Deactivation of NO(v=1) by Molecular Oxygen at Room Temperature 6
      3.3.3 Measurement of the Deactivation of NO(v=1) by Nitrogen Dioxide at Room Temperature 6
      3.3.4 Measurement of the Deactivation of NO(v=1) by Atomic Oxygen 7
4. Measurement of the Deactivation of $CO_2(01^10)$ 8
   4.1 Background. 9
   4.2. Experiment. 9
      4.2.1 Pressure and Temperature Measurements 9
      4.2.2 Detection of Vibrationally-excited CO_2 9
      4.2.3 Data Collection and Analysis 10
      4.2.4 Measurement of the Absolute Concentration of Atomic Oxygen 10
      4.2.5 Measurement of Flow Rates 10
      4.2.6 Gas Purity 10
   4.3. Results 10
      4.3.1 Measurement of the Vibrational Distribution of CO_2 10
      4.3.2 Preliminary Experiments to Measure CO_2 Deactivation by Atomic Oxygen 13
      4.3.3 Measurement of the Deactivation of $CO_2(01^10)$ by Helium and Argon and Oxygen 14
         4.3.3.1 Preliminary Experiments 14
         4.3.3.2 Measurement of the Deactivation of $CO_2(01^10)$ by Helium and Argon 14
         4.3.3.3 Measurement of the Deactivation of $CO_2(01^10)$ by Atomic Oxygen 15
5. Conclusions 16
6. References 17
7. Appendix 19

Figures

1. Schematic of the apparatus used to measure the deactivation of NO(v=1) 3
2. Calculation showing the overlap between the P(11)8→7 CO laser line and the Doppler broadened NO($^2\Pi_{1/2}$) (R12.5) doublet 4
3. Variable temperature flow reactor 5
4. Typical NO(v=1) fluorescence signal 6
5. Deactivation of NO(v=1) by O_2 6
6. Deactivation of NO(v=1) by NO_2 7
7. Deactivation of NO(v=1) by O 7
8. Temperature dependence of the deactivation rate of NO(v=1) by O 8
9. Schematic of the apparatus used to measure the deactivation of $CO_2(01^10)$ 9
10. Vibrational energy diagram of CO_2 10
11. Spectrum of discharged CO_2 near 2307 cm^{-1} 12
12. Preliminary experiments to determine the deactivation of $CO_2(01^10)$ by O 13
13. The deactivation of $CO_2(01^10)$ by He and Ar 15
14. The deactivation of $CO_2(01^10)$ by O 15

Tables

1. CO_2 vibrational transitions near 2307 cm^{-1} 11
2. Assignments of spectroscopic lines near 2307 cm^{-1} 12
3. Intensities and calculated densities of assigned lines in discharged CO_2 13
4. Results of preliminary deactivation experiments using new procedure 14
5. Species concentrations for the experiments to determine the deactivation of CO_2 (01^10) by He and Ar 14
6. Species concentrations for the experiments to determine the deactivation of CO_2 (01^10) by O 15

1. Summary

Spectral measurements of the limb radiation of the earth have shown that emissions from the NO(v=1) and $CO_2(01^10)$ states dominate the nighttime radiance seen at long wavelengths. At the high altitudes of the thermosphere, the deactivation of the aforementioned molecules helps regulate the temperature. A knowledge of the kinetics of deactivation of these molecules is therefore needed to accurately model the temperature of the thermosphere.

Sharma and coworkers have developed a procedure to invert the profiles of the limb emissions to determine the vertical distributions of local atmospheric properties.[1-5] This procedure can be used to monitor local NO, NO(v=1), CO_2 and O densities as well as translational temperatures. They have shown the inversion procedure is sensitive to the rate of the reaction for deactivation of NO(v=1) and $CO_2(01^10)$ by O atoms.

Before the start of the present study, the only laboratory determinations of the rate of deactivation of NO(v=1) by O were a study at room temperature and another near 3000°C. There were no determinations for the rate for deactivation of $CO_2(01^10)$ by O.

We constructed an apparatus to measure the rate of deactivation of NO(v=1) by O. The apparatus consisted of a pulsed CO electric discharge laser which was used to excite NO to its first vibrational state, a fast-flow reactor to deliver atomic oxygen to the NO flow, a microwave generator to produce O, an EPR detector to measure O concentrations, and an infrared detector to monitor the emission from the NO(v=1). Using this apparatus, we determined the rate constant for the deactivation of NO(v=1) by O to be $5\pm1\times10^{-11}$ $cm^3molecule^{-1}s^{-1}$ in the temperature range 200-350K .

We subsequently constructed a second apparatus to measure the deactivation of $CO_2(01^10)$ by O. This apparatus consisted of a large diameter fast flow reactor to maintain a measurable flow of vibrationally-excited CO_2, two microwave discharges, the first to excite the CO_2 and the second to dissociate O_2 into O-atoms, an NO_2 titration system to measure O concentrations, and a laser diode spectrometer to monitor the vibrationally-excited states of CO_2. We used this apparatus to measure the rate constant of deactivation of $CO_2(01^10)$ by O. The rate at 301K was determined to be $5\pm2\times10^{-13}$ $cm^3molecule^{-1}s^{-1}$.

2. Introduction

This report presents the results of a study to obtain the rates of deactivation of the important temperature regulating reactions of the thermosphere. This study was initiated after the launch of the Spectral Infrared Rocket Experiment (SPIRE) showed the NO(1→0), (NO*) band near 5 μm and the $CO_2(01^10)\rightarrow(00^00)$, ($CO_2$*) band near 15 μm are the dominant features in the nighttime radiance seen at infrared long wavelengths.

In a series of papers, Sharma and coworkers have shown that the profiles of the earth's infrared limb emissions can be analyzed to obtain vertical distributions of local atmospheric properties.[1-5] They described an inversion procedure that allows recovery of both upper and lower state densities and translational temperatures. In subsequent work they have shown that limb spectral radiance profiles such as those produced by SPIRE can be used to monitor local NO, NO^*, CO_2^* and O densities as well as translational temperatures provided accurate measurements of the rate constant for the key deactivation processes are known.[3,5]

At the low pressures encountered in the thermosphere, thermal equilibrium among all species is not assured. A species such as NO can be deactivated or excited by collisions with other molecules via the equilibrium process,

$$NO^* + M \leftrightarrow NO + M. \quad (1)$$

It can also lose energy by radiation via the process,

$$NO^* \rightarrow NO + h\nu. \quad (2)$$

Radiative losses such as reaction (2) cool the atmosphere, whereas reactions such as (1) retain energy. Reactions (1) and (2) help regulate the temperature of the thermosphere and therefore

their rates are important for atmospheric modeling.

At the altitudes of the thermosphere, atomic oxygen is the dominant deactivating species. At the start of the present effort, the only laboratory data for the rate constant of deactivation of NO* by atomic oxygen in the range of interest of the thermosphere was at room temperature. In addition, there was no laboratory data for the deactivation of $CO_2(01^10)$ by atomic oxygen. The present experiments were initiated to obtain laboratory data for these reactions.

3. Measurement of the Deactivation of NO(v=1)

Kockarts suggested the importance of NO in regulating the temperature of the thermosphere.[6] His modeling indicated that above 120 km, the deactivation by the reverse reaction in the equilibrium,

$$NO(v=0) + M \leftrightarrow NO(v=1) + M, \qquad (3)$$

is much slower than the emission,

$$NO(v=1) \rightarrow NO(v=0) + h\nu. \qquad (4)$$

Therefore the IR emission from NO(v=1) is never in local thermodynamic equilibrium at these altitudes.

Subsequent measurements by the Spectral Infrared Rocket Experiment, showed the NO(1→0) band at 5.3 μm is a dominant feature in the nighttime radiance seen at long wavelengths.[4] Profiles of the earth's infrared limb emissions can be analyzed to obtain vertical distributions of local atmospheric properties. Zachor and coworkers have described an inversion procedure that allows recovery of both upper and lower state densities and translational temperatures.[5] In subsequent work they have shown that limb spectral radiance profiles such as that produced by SPIRE can be used to monitor local NO, NO* and O densities as well as translational temperatures provided an accurate measure of the rate constant for the deactivation process,

$$O + NO(v=1) \rightarrow O + NO(v=0), \qquad (5)$$

is used. This study was undertaken to obtain reliable temperature dependent data for the rate of this reaction.

3.1 Background. The rate constant for the deactivation of NO(v=1) by atomic oxygen has been the subject of two experimental investigations.[7,8] The first of these investigations involved an indirect measurement of the rate constant at room temperature, while the second involved a shock-tube measurement at high temperature. Of these two, only the room temperature measurement is in the temperature range of significance to modeling of the upper atmosphere. The room temperature measurement was made using a hydrogen chloride chemical laser to excite HCl to its first vibrationally-excited state. The HCl(v=1) then transferred energy to NO via the process,

$$HCl(v=1) + NO(v=0) \rightarrow HCl(v=0) + NO(v=1). \qquad (6)$$

This technique, which uses an indirect method of exciting the NO, requires a more complex and less straight-forward analysis than a technique employing direct excitation. Therefore it appears a more direct approach to determination of this deactivation rate is warranted.

Stephenson and Freund used a CO laser in combination with a flow tube reactor to excite NO to the v=1 state.[9] They used a magnetically shifted P(13) transition in the CO 9→8 band to measure the rate of deactivation of NO(v=1) by O_3. Other workers have shown the 8→7 P(11) transition of CO overlaps within the Doppler width of one of the $^2\Pi_{1/2}$, J=25/2 R branch doublets in NO.[10] In our work we used the latter technique to make NO(v=1) and measured the rate of quenching of NO(v=1) by atomic and molecular oxygen and nitrogen dioxide.

3.2. Experiment. The experimental configuration used in this work is shown in Figure 1. As shown, a flow tube was employed to deliver the reactants to a variable-temperature reactor where the deactivation was monitored in real time using the fluorescence from NO(v=1).

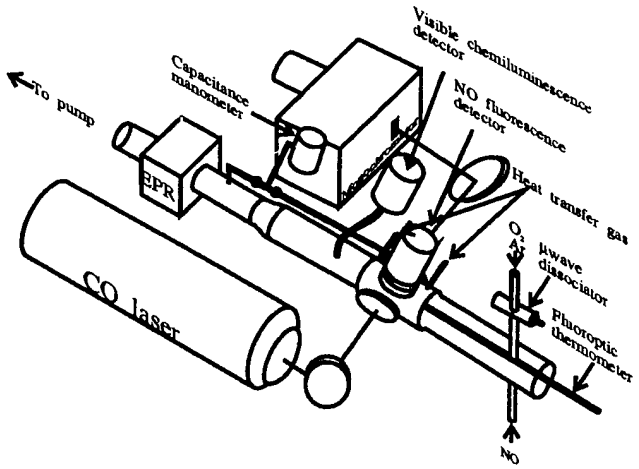

Figure 1. Schematic of the apparatus used to measure the deactivation of NO(v=1).

A stream of O_2 in Ar carrier gas flowed through a microwave-discharge to produce atomic oxygen approximately 15 cm upstream of the observation port. NO was added to the effluent of the discharge through an injector located downstream of the discharge region. A beam from a pulsed-discharge CO laser was used to promote the NO to its first excited vibrational state. The laser beam crossed the stream containing the O_2, O, Ar and NO mixture perpendicular to the flow. The rate of decay of NO(v=1) fluorescence near 5 μm was monitored using an InSb detector that viewed the radiation in a direction perpendicular to both the flow direction and the laser excitation direction. The flow then traversed an EPR cavity where the absolute concentration of atomic oxygen was determined prior to the flow being exhausted to a mechanical pump.

3.2.1 Flow Measurements. Except for NO_2, the flows of all gases used were regulated and measured using mass flow controllers which were periodically calibrated by flowing the gases into a known volume. The flow rates were derived by monitoring the rate of pressure increase into the known volume with a capacitance manometer. The NO_2 flow was regulated by a standard leak valve and was measured after each experiment by flowing the gas into the known volume. The flow rates of reactants were varied from experiment to experiment. Typical pressures in the reactor ranged from 1-4 Torr and typical flow velocities ranged from 100-1000 cm/s.

3.2.2 Production and Measurement of Atomic Oxygen. The atomic oxygen was monitored during the course of the experiments using the emission from the O + NO reaction. This reaction has been studied in our flow reactor and in other systems (Ref. 11 and references contained therein). The emission is known to originate from the following set of reactions,

$$O + NO \rightarrow NO_2^* \text{ (slow)}, \quad (7)$$

$$NO_2^* \rightarrow NO_2 + h\nu, \quad (8)$$

$$NO_2^* + M \rightarrow NO_2 + M, \quad (9)$$

$$NO_2 + O \rightarrow NO + O_2 \text{ (rapid)}, \quad (10)$$

where NO_2^* denotes an excited state of NO_2. The emission intensity of this reaction is proportional to both the atomic oxygen and the nitric oxide concentration. Because of the rapid reaction (10), the nitric oxide consumed by the slow reaction (7) is rapidly regenerated and its concentration does not change with time as long as atomic oxygen is present. Thus changes in the emission from NO_2^* represent changes in the atomic oxygen concentration under our experimental conditions. As shown in Figure 1, a photomultiplier with a 10 nm filter centered at 540 nm and a fiber optic was used to monitor the visible chemiluminescence at various positions in the flow tube. During the decay measurements, the fiber optic was positioned to determine the atomic oxygen concentration at the same point in the reactor that the decay measurements were made.

For the room temperature measurements, the chemiluminescence detector was calibrated using EPR. In these calibrations, the EPR signal from the atomic oxygen is compared with the ground state signal obtained from a known density of O_2 . The details of the EPR measurement technique have been described by Westenberg and de Haas[12,13] and this technique has been employed by us on numerous occasions.[11,14,15] The fluorescence signal from the O + NO reaction obtained both before and after the EPR cavity was averaged and compared with the measured atomic oxygen density. The known

oxygen density together with the NO density (determined from the measured flow rates and total pressure), provided a room temperature calibration of the chemiluminescence detector.

For the non-ambient experiments, the flow reactor and EPR are at distinctly different temperatures. Correction for the temperature differences between the cavity and the reactor would add considerable uncertainties to the determination of the atomic oxygen concentration. We therefore chose to titrate the atomic oxygen with NO_2 to determine atomic oxygen concentrations at non-ambient temperatures. Titration is a standard technique employed by many workers to measure atomic oxygen concentrations.[16] It has been extensively compared with the EPR technique and the two have been shown to be in excellent agreement.[12] In addition, we performed an experiment at room temperature comparing the two techniques in our system and found them to agree within 10%. The NO_2 titration technique employs reactions (7) to (10) for measurement of atomic oxygen. As long as atomic oxygen is present in the flow, the addition of NO_2 will be accompanied by the O + NO visible chemiluminescence. When the amount of NO_2 added to the flow equals the atomic oxygen concentration, the oxygen atoms will be reacted completely with NO_2 in the fast reaction (10). At this endpoint there will be no atomic oxygen available to produce the chemiluminescence and the flow tube will become dark downstream of the mixing zone.

For these calibrations NO_2 was injected into the flow stream at a point just upstream of the flow reactor. The endpoint of the reaction was determined 10 cm downstream from the flow reactor.

3.2.3 Excitation of NO(v=1). The P(11)8→7 line of CO is coincident with one of the NO R(12.5) lines within its Doppler width as shown in Figure 2. The displacement of this CO line from the line center of the NO transition at room temperature was calculated using the data from Ref.17.

The formation of atomic oxygen via microwave discharge is only experimentally practical at pressures below 20 Torr. Accurate measurement of deactivation of NO(v=1) by atomic oxygen requires us to work under conditions where

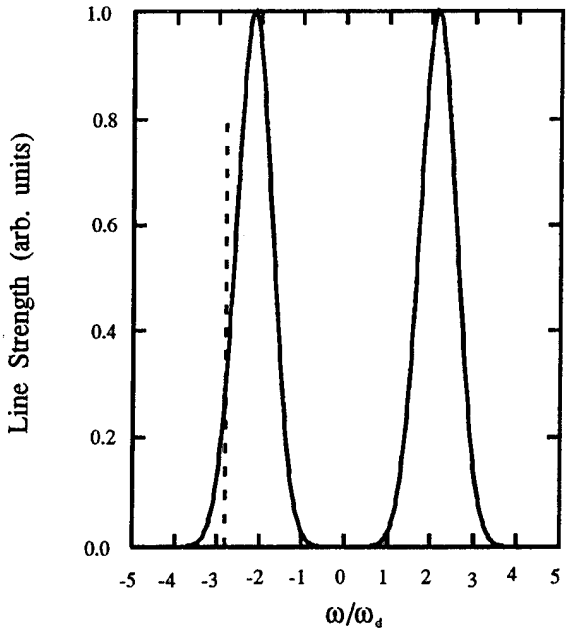

Figure 2. Calculation showing the overlap between the P(11)8→7 CO laser line (dashed) and the Doppler broadened NO($^2\Pi_{1/2}$) (R12.5) doublet. ω_d is the full width at half height of the NO lines.

atomic oxygen is the dominant deactivator in the flow. This limits the maximum density of NO in the flow stream to pressures less than 1 Torr. Thus it is important to find a coincidence line between CO and NO without having to pressure broaden the NO absorption line. The transition used in this work is one of a very few coincidences that meets this stringent criterion.

A pulsed, longitudinal flow CO electric discharge laser was therefore assembled next to the reactor tube. A pin discharge 180 cm in length and perpendicular to the flow axis was used to excite the CO. The discharge excited the CO to a high vibrational level (v=8). After an inversion was established, the CO lased from this high vibrational state with $\Delta v=-1$ and $\Delta J=\pm 1$. Subsequently, an inversion was created in the next lower vibrational level and it also lased. This cascade produced output on dozens of lines in each vibrational level. The time delay of any particular line after the electric discharge pulse was determined by the initial distribution produced in the discharge and the kinetics in the laser cavity. Output on the P(11)8→7 line was

enhanced by placing a grating in the cavity of the laser outside of the section containing the flowing CO. The section of the laser containing the grating was purged with dry nitrogen to minimize absorption of the P(11) 8 →7 transition by water vapor. The total time delay for lasing was less than 10 μs.

After traversing the reactor cell, the attenuated laser radiation was passed through a 0.25 meter monochromator to an InSb detector. In this manner the laser intensity was monitored during the course of an experiment. The time response of the laser and detector system was faster than 10 μs. Most of our data was taken for decays slower than 100 μs where neglecting the finite response time of the system accounted to an error of less than 10%.

3.2.4 Temperature Regulation. For experiments performed at temperatures below ambient, the reactor was cooled by passing the boiloff from a liquid nitrogen tank through an outer jacket on the flow reactor (see Figure 3). The temperature was regulated by heating the nitrogen before it entered the jacket. For experiments performed above ambient temperatures, preheated nitrogen gas was flowed through the outer jacket to heat the reactor.

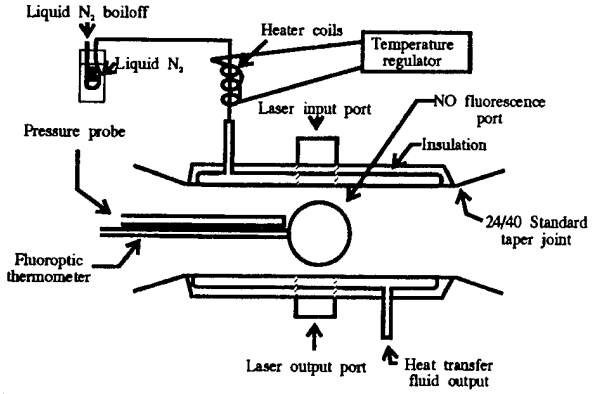

Figure 3. Variable temperature flow reactor. The reactor is shown for temperatures below ambient. For above ambient operation the nitrogen source was a high pressure cylinder.

The temperature of the reacting flow stream was measured using a fluoroptic thermometer (Luxtron Model 100A with a low temperature probe/EPROM) and the pressures were determined using a capacitance manometer (Baratron model 315).

3.2.5 Data Collection and Analysis. The signal from the infrared detector was directed to a Tektronix 2440 digital storage scope where 256 shots were averaged. The averaged signal was then taken via a GPIB bus to a Digital VAXLab computer where it was stored and analyzed. The software used to analyze the signal was written in FORTRAN using VAXLab I/O to interface the scope and VAXLab graphics routines to display the data. The analysis routines incorporated subroutines to further average the data (averaging multiple ensembles of 256 shots), baseline correction routines and a nonlinear least squares routine with statistical analysis.

The nonlinear least squares routine, LMDER, was taken from the MINPAC subroutine package. This package was developed by Argonne National Laboratory.[18] LMDER minimizes the sum of the squares of M nonlinear functions in N variables by a modification of the Levenberg-Marquardt algorithm, given a user-supplied subroutine that evaluates the functions and the Jacobian matrix.

We fit our data to a functional form,

$$I = A*\exp(-B*t) + C, \qquad (11)$$

which represents a single exponential decay with a baseline offset, C.

The program iterates solutions to equation (11) and calculates the parameters A, B, and C as well as the statistical uncertainty of these parameters. The parameter B, which represents the exponential decay rate of the NO(v=1) signal is the parameter of experimental interest. The parameter B and its statistical uncertainty were used to calculate the rate constant, k, for deactivation of NO(v=1) and the 90% confidence level for the error in k. All of the data taken were analyzed using this procedure.

3.3 Results. Experiments were performed to determine the rate of deactivation of the first vibrationally-excited state of NO by O_2, NO_2 and atomic oxygen.The results of these experiments are described below.

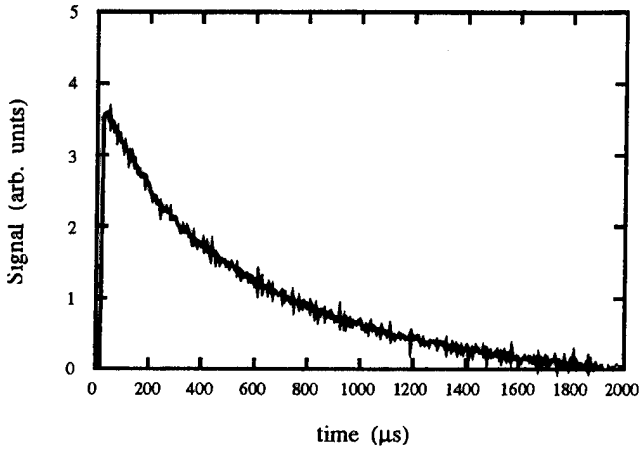

Figure 4. Typical NO(v=1) fluorescence signal.

3.3.1 Operation of the CO Laser on the P(11)8→7 line. The output of the laser was characterized to identify the lines lasing at frequencies near 1917.8 cm^{-1}. The laser beam was passed through a 12 cm long attenuation cell filled with 100 Torr of NO, prior to traversing a 0.25 meter monochromator and an InSb detector. An approximate calibration of the monochromator was obtained by observing high-order spectra of a He-Ne laser. A more precise calibration was obtained by monitoring the signals from the P(13) 7→6 and P(15) 7→6 lines of the CO laser that have known frequencies of 1935.4819 and 1927.2959 cm^{-1} respectively.[10] These lines were identified in the complex output spectra of the CO laser by attenuating the laser output with 100 Torr of NO in the attenuation cell. The P(13) and P(15) lines of the 7→6 vibrational band of the CO laser are the only two lines in this spectral region that are significantly attenuated by NO. The P(11) 8→7 line was then found by tuning the grating while examining the output of the laser near 1917.86 cm^{-1}. The identity of the transition was confirmed by attenuation of the line with submillimeter pressures of NO.

3.3.2 Measurement of the Deactivation of NO(v=1) by Molecular Oxygen at Room Temperature. Measurements of the deactivation of NO(v=1) were made at several partial pressures of O_2. The flow rate of the oxygen was varied while holding the partial pressures of the other gases (NO and Ar) in the reactor fixed. A typical decay of NO(v=1) obtained in this manner is shown in

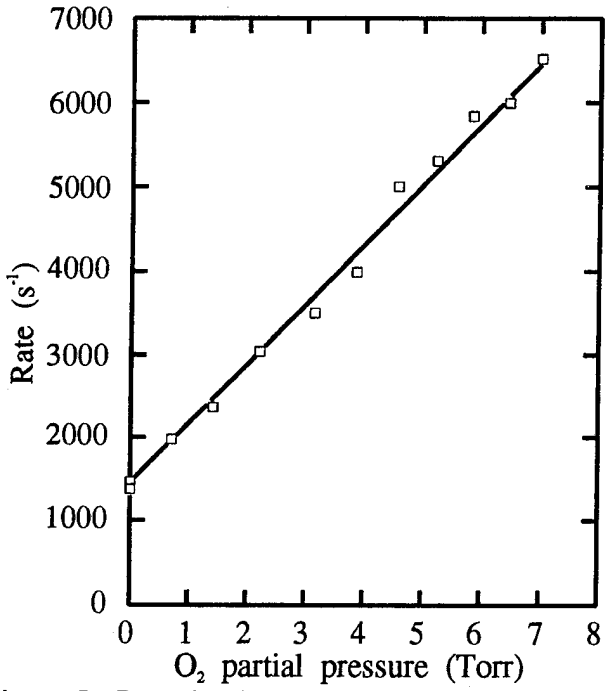

Figure 5. Deactivation of NO(v=1) by O_2.

Figure 4. The total deactivation of NO(v=1) is equal to the sum of all of the deactivation processes present. In this experiment, that includes O_2, Ar and NO. The rates were then plotted as a function of O_2 density and these results are shown in Figure 5. The slope of the line obtained in Figure 5 represents the deactivation rate by O_2. The intercept of the line is the sum of all other deactivation rates, including collisions with the wall and other gases as well as the radiative decay [(reaction (8)]. The rate constant obtained from the slope, $k = (2.3\pm0.3)\times10^{-14}$ $cm^3molecule^{-1}s^{-1}$, is in reasonably good agreement with the value obtained, $k = (2.9\pm0.3)\times10^{-14}$ $cm^3molecule^{-1}s^{-1}$, in a previous determination by Stephenson and Freund[9] and that obtained by Green et. al.[19], $k=(2.4\pm1.5)\times10^{-14}$ $cm^3molecule^{-1}s^{-1}$.

3.3.3 Measurement of the Deactivation of NO(v=1) by Nitrogen Dioxide at Room Temperature. Measurements of the deactivation of NO(v=1) by NO_2 were made by adding NO_2 to a flowing mixture of NO and Ar. As above, the NO_2 flow was varied while holding the partial pressures of the other constituents constant. The data analysis for these experiments was similar to that described above for the O_2 deactivation

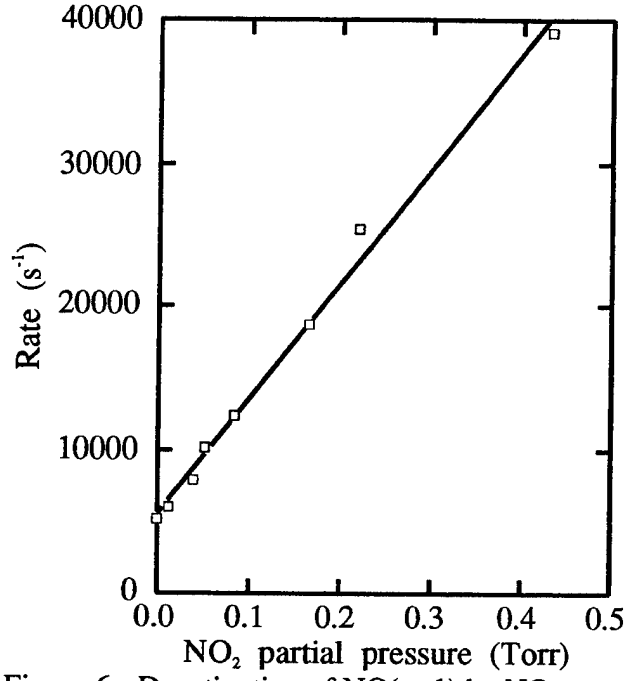

Figure 6. Deactivation of NO(v=1) by NO_2.

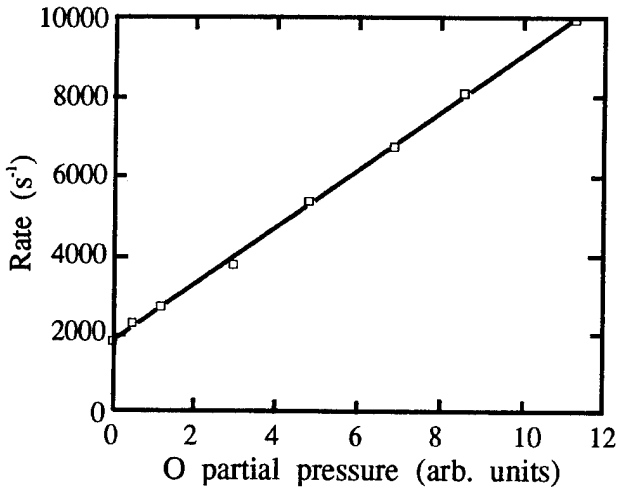

Figure 7. Deactivation of NO(v=1) by O.

experiments. Typical results for the deactivation rate as a function of NO_2 density are show in Figure 6. The average rate constant for deactivation of NO(v=1) by NO_2 over the course of five experimental determinations was $(2.5 \pm 0.2)\times10^{-12}$ $cm^3molecule^{-1}s^{-1}$, where the quoted error represents the statistical uncertainty at the 90% confidence level. This value is in good agreement with the value obtained by Stephenson, $k = 2.2\pm0.2\times10^{-12}$ $cm^3molecule^{-1}s^{-1}$.[20]

3.3.4 Measurement of the Deactivation of NO(v=1) by Atomic Oxygen. Atomic oxygen was generated in these experiments as previously described (see Figure 1). NO was added to the flow through the injector located upstream of the temperature controlled reactor. The atomic oxygen concentration was varied by adjusting the power to the discharge. The atomic oxygen concentration in the reactor was measured using the calibrated photomultiplier detector described above. The deactivation of NO(v=1) was measured as a function of atomic oxygen pressure. Figure 7 shows a typical plot of the deactivation of NO(v=1) vs. atomic oxygen pressure.

The analysis of these experiments is somewhat more complicated than the analysis for the deactivation by O_2 and NO_2. Production of atomic oxygen in a microwave discharge is a well-studied process (Ref. 13 and references cited therein). The percentage of the O_2 dissociated is a function of the discharge power, with the atomic oxygen concentration maximizing at about 10% of the O_2 flow at powers near 100 watts. The ground state O_2 density is depleted as the microwave power is increased through excitation and dissociation processes, to a level of approximately 90% of its initial density. Thus, it is technically not possible to keep the O_2 concentration fixed when varying the atomic oxygen concentration using the discharge power. As will be shown, however, the deactivation rate of NO(v=1) by O is more than three orders of magnitude larger than the deactivation by O_2. Therefore ignoring the variation in O_2 partial pressure during the variation of the microwave power results in an error of 0.1% in the determination of the rate constant for deactivation by atomic oxygen.

Another complication in our experiments is caused by the fact that discharges produce $O_2(^1\Delta)$ at concentrations up to about 10% of the flow and much smaller amounts (<1% of the flow) of $O_2(^1\Sigma)$, $O(^2D)$ and $O(^2P)$. The latter three species are in such small concentrations in the flow that their rate for deactivation for NO would have to be more than 100 times faster than gas kinetic to compete equally with atomic oxygen for deactivation of NO(v=1) under our ex-

perimental conditions. If the rate for deactivation of NO(v=1) by $O_2(^1\Delta)$ were greater than 10^{-13} $cm^3molecule^{-1}s^{-1}$, however, it could plausibly compete with atomic oxygen for NO deactivation.

We therefore performed an experiment where the discharged flow was titrated with NO_2 to remove all of the atomic oxygen present. NO_2 reacts rapidly with atomic oxygen via reaction (5) but does not remove $O_2(^1\Delta)$, $O_2(^1\Sigma)$, $O(^2D)$ or $O(^2P)$. At the endpoint of the titration of O with NO_2, all of the reactants are consumed while NO and O_2 are produced. If 5% of the O_2 in the discharge is dissociated and the atomic oxygen produced is titrated with NO_2, the net result is an addition of 10% NO and 5% O_2 to the oxygen flow. The rate constants for deactivation of NO(v=1) by both O_2 and NO are small (2 and $8x10^{-14}$ $cm^3molecule^{-1}s^{-1}$, respectively) when compared with the rate constant for deactivation by atomic oxygen. Therefore the contribution of the additional O_2 and NO produced by the titration to the relaxation is small (200 s^{-1}) when compared with the deactivation of undischarged O_2 (~ 2000 s^{-1}, as in Figure 6) .

By the arguments given above, if the increase in deactivation of NO(v=1) seen in discharged O_2 (Figure 7) is caused by deactivation by atomic oxygen, the deactivation observed after the discharge and subsequent NO_2 titration, should be comparable to that observed with the discharge off. If, however, the deactivation was caused by a species that is not effected by the titration ($O_2(^1\Delta)$ for example does not react with NO_2) the deactivation observed after the discharge and subsequent NO_2 titration should be comparable to that observed with the discharge on.

When atomic oxygen was removed in this fashion the rate of deactivation of NO(v=1) decreased to a rate comparable to that observed when the discharge was turned off. This result indicates atomic oxygen is the primary deactivator in discharged O_2.

The deactivation of NO(v=1) by atomic oxygen was investigated in the temperature range between 200-350K. The results are shown in Figure 8. Also shown in Figure 8 are the results of other workers who have investigated this reaction.

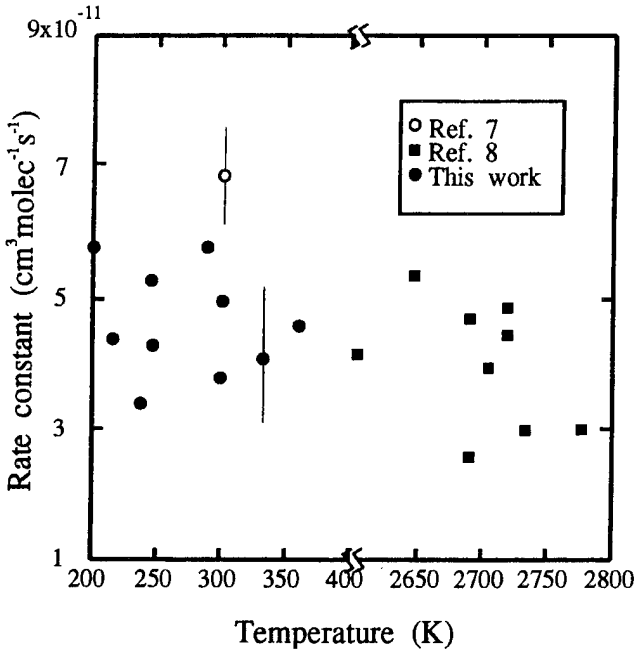

Figure 8. Temperature dependence of the deactivation rate of NO(v=1) by O.

Our experiments show a fast deactivation rate, $(5\pm1)x10^{-11}$ $cm^3molecule^{-1}s^{-1}$, with little temperature dependence in the range 200-350K. The temperature dependence is in good agreement with the high temperature results of Glanzer and Troe taken around 2700K which cluster about a value of $4x10^{-11}$ $cm^3molecule^{-1}s^{-1}$. Our room temperature value is in reasonable agreement with the room temperature value $(6.5\pm0.7)x10^{-11}$ $cm^3molecule^{-1}s^{-1}$ reported by Fernando and Smith.

4. Measurement of the Deactivation of $CO_2(01^10)$

Sharma and Nadile have developed a non-equilibrium model to understand the limb radiance observed from rocket borne experiments.[1] They have successfully used this model to explain the observations of the $CO_2(01^10)\rightarrow CO_2(00^00)$ radiation at 15 μm for altitudes between 50 and 150 km. Their model uses a room temperature rate of deactivation of $CO_2(01^10)$ of $5x10^{-13}$ $cm^3molecule^{-1}s^{-1}$. This reaction rate is central to the Sharma and Nadile model in that the deactivation of $CO_2(01^10)$ is

dominated by atomic oxygen at heights above 95 km.

4.1 Background. At the start of the present investigation the only laboratory data for the deactivation of $CO_2(01^10)$ by atomic oxygen was a high temperature investigation by Center in the range between 2000-4000K.[21] His experiment showed the deactivation to be about an order of magnitude faster than deactivation by Ar. This yielded a rate of about $3x10^{-13}$ $cm^3molecule^{-1}s^{-1}$ in this high temperature region.

Recently, Shved and coworkers have made a measurement of the deactivation rate of $CO_2(01^10)$ by atomic oxygen at room temperature by modeling a hallow cathode gas discharge in pure CO_2.[22] They report a very fast rate for deactivation of $\sim 1x10^{-12}$ $cm^3molecule^{-1}s^{-1}$. Their method of determination involved simultaneous modeling of five reaction rates but no error analysis was performed.

4.2. Experiment. The experimental apparatus used for these experiments is shown in Figure 9. This system employed a 2000 cfm pump and a large diameter (2") flow tube to minimize wall deactivation and still maintain the fast flow velocity needed to perform these experiments.

Vibrationally-excited CO_2 was formed by flowing CO_2 through a microwave discharge. The effluent from the discharge passed into the flow reactor through a transverse injector located near the first observation port. Atomic oxygen was formed by flowing O_2 through a second microwave discharge. The oxygen stream entered the flow reactor through an injector located a distance of 1 cm upstream from the center of the first optical port. The carbon dioxide and oxygen streams mixed and the resultant stream flowed through the reactor traversing three additional observation ports before being exhausted to the pumping system.

4.2.1 Pressure and Temperature Measurements. The temperature of the flow stream was monitored continuously using a thermocouple located at the second observation port (see Figure 9). The pressure of the flow stream was measured using a capacitance manometer.

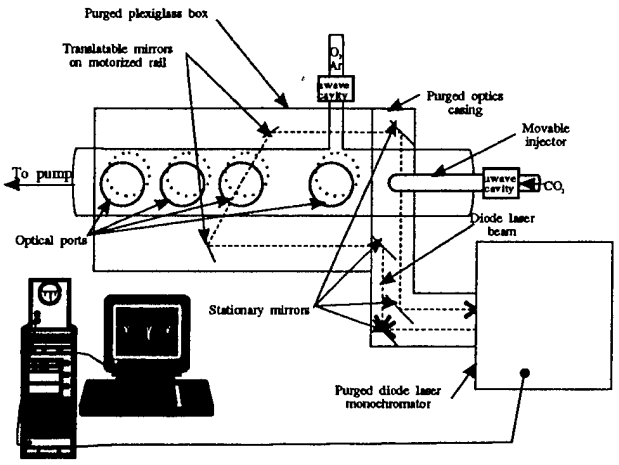

Figure 9. Schematic of the apparatus used to measure the deactivation of $CO_2(01^10)$.

4.2.2 Detection of Vibrationally-excited CO_2. CO_2 transitions of the type $(v_1v_2^l,v)\rightarrow(v_1v_2^lv_3+1)$ were detected using a Laser Analytics diode laser spectrometer operating near 2307 cm^{-1}. The spectrometer consisted of the laser diode, a monochromator to restrict operation of the laser to a single mode, a HeNe alignment laser, an etalon for calibration purposes, an InSb detector and associated optics and mirrors. After exciting the laser diode, the optical beam was modulated at 200 Hz using a vibrating chopper. The beam was then directed by mirrors through an enclosed path to one of the calcium fluoride optical ports located on the flow reactor. It subsequently traversed the flow reactor in a direction parallel to the flow axis and exited through a second calcium fluoride optical port. A similar optical train was then used to direct the beam back into the monochromator where it was monitored using an InSb detector. The entire path of the beam from the laser to the detector was enclosed in a sealed Plexiglas® box and purged with dry air that had been passed over Ascarite® pellets to remove CO_2. As shown in Figure 9, the two mirrors in the optical train that directed the beam entering and exiting the flow reactor were mounted on a motorized optical rail. The optical rail was computer controlled to allow the operator to position the mirrors so that the beam could traverse the flow reactor at any of the four optical ports on the system.

4.2.3 Data Collection and Analysis. The signal from the infrared detector was directed to a Tektronix 2440 digital storage scope. The ramp signal which was used to scan the diode laser frequency was also used as the x input to the scope. In this manner a spectrum of the laser diode signal was obtained. As described above, the optical signal was modulated mechanically by a 200 Hz chopper. Thus, the true zero for the optical signal was continually monitored and averaged. The averaged signal was then taken via a GPIB bus to a Digital VAXLab computer for analyzing and storing.

4.2.4 Measurement of the Absolute Concentration of Atomic Oxygen. The atomic oxygen concentration was measured using the NO_2 titration technique. This technique was described in detail in Section 2.

4.2.5 Measurement of Flow Rates. The flow rates of all species of interest except NO_2 were measured with calibrated flow meters (Tylan). The NO_2 flow was measured directly by flowing the gas into a calibrated volume.

4.2.6 Gas Purity. All of the gases used were 99.99% pure and contained less than 4 ppm of H_2O. The oxygen, argon and helium were passed through a dry ice/ethanol trap before entering the flow reactor.

4.3. Results. Experiments were performed to measure the room temperature rate of deactivation of $CO_2(01^10)$ by He, Ar and O. The results of these experiments are described below.

4.3.1 Measurement of the Vibrational Distribution of CO_2. Figure 10 shows a simplified diagram of the important vibrational modes of CO_2. When CO_2 is discharged, a number of these vibrational levels are excited. As shown in Figure 10, the (001) and (030) modes are strongly coupled, as are the (100) and (020) modes. Thus the relaxation kinetics of CO_2 excited in a discharge are very complicated. Fortunately, because of the importance of CO_2 discharge lasers, the kinetics of relaxation of CO_2 has been well studied. Bailly and coworkers have examined the infrared emissions from discharge-excited CO_2 and have fit the vibrational distributions to Boltzmann and Treanor

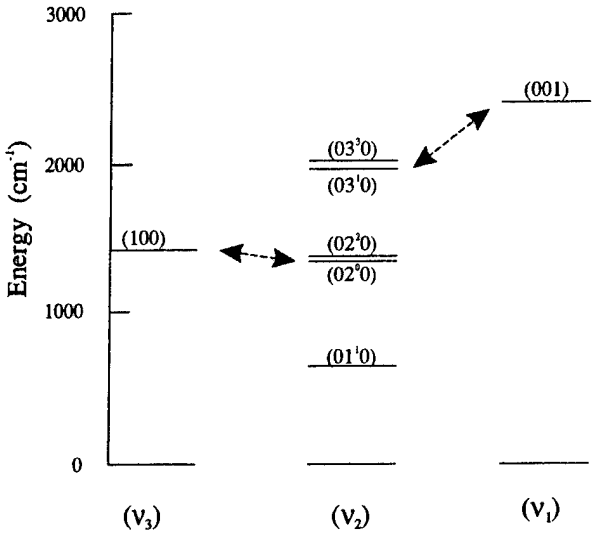

Figure 10. Vibrational energy diagram of CO_2.

models.[23] They found that the major levels populated by the discharge technique (>1%) are : (00^01), (00^02), (01^10), (01^11), (02^20), (02^21), $(10^00)_I$, $(10^00)_{II}$, $(10^01)_I$, $(10^01)_{II}$ and (02^20) (where the I and II subscripts represent the Fermi polyads in their notation). As these levels relax, v-v relaxation processes tend to be very fast, and after some time, the (00^01) and (00^00) levels are enriched relative to the other levels. The simplest model for v-t relaxation that could be invoked for these conditions involves consideration of only the two lowest levels, i.e.,

$$CO_2(01^10) + M \leftrightarrow CO_2(00^00) + M. \qquad (12)$$

The backward reaction must be considered for this case since the (01^10) state is significantly populated even at room temperature. The kinetics of this process can therefore be described by,

$$d[CO_2(01^10)]/dt = -k_1[M][CO_2(01^10)]$$

$$+ k_{-1}[M][CO_2(00^00)]. \qquad (13)$$

The solution for the rate of formation of CO_2 (01^10) is,

$$\{[CO_2(01^10)] - [CO_2(01^10)]_e\}/$$

$$\{[CO_2(01^10)]_0 - [CO_2(01^10)]_e\}$$

$$= \exp\{-(k'_1+k'_{-1})t\}, \qquad (14)$$

where $k' = k[M]$, the subscript 0 represents the concentration at t=0 and the subscript e represents the concentration at equilibrium. The quantity, $\{[CO_2(01^10)]_0 - [CO_2(01^10)]_e\}$, would thus decrease exponentially as a function of time under these conditions. If the kinetics were to involve more than one level, for example the 02^00 level, the kinetics would be more complicated by the additional reactions,

$$CO_2(02^00) + M \leftrightarrow CO_2(01^10) + M. \qquad (15)$$

Under these conditions the kinetics would involve two coupled equations and four concentrations of vibrational states of CO_2.

Our first task then was to determine the relative concentrations of vibrationally excited species under our experimental conditions to determine the appropriate model to use for analysis.

The diode laser used in our experiments to detect vibrationally-excited CO_2, operates at wavelengths near 5 μm. In this region we can detect CO_2 transitions of the type, $(v_1,v_2^l,v_3)\rightarrow(v_1,v_2^l,v_3+1)$, where v_1, v_2 and v_3 are the three vibrational modes of the ground electronic state of CO_2. As a preliminary to determining the concentrations of vibrationally excited CO_2, we calculated the energies of the transitions that were likely to be populated under our experimental conditions. For these calculations we used the spectroscopic constants determined by D. Bailly and coworkers[24,25] to determine the P- and R-branch energies for the vibrational transitions, $(00^00\rightarrow00^01)$, $(00^01\rightarrow00^02)$, $(00^02\rightarrow00^03)$, $(01^10\rightarrow01^11)$, $(01^11\rightarrow01^12)$, $(02^20\rightarrow02^21)$, $(02^21\rightarrow02^22)$, $(03^30\rightarrow03^31)$, $(10^00\rightarrow10^01)$, $(10^01\rightarrow10^02)$, $(02^00\rightarrow02^01)$, and $(02^01\rightarrow02^02)$. The detailed results of these calculations are included as an appendix to this report.

The spectroscopic range of interest for our diode spectrometer occurs between 2306-2308 cm^{-1}. The transitions in this range are shown in Table 1. Some of the lines listed in Table 1 have been tabulated by Guelachvili and Rao.[25] The positions of these lines were compared with those in Ref. 25 and were found to agree within 0.001 cm^{-1}. (In Ref. 25, the notation for the Fermi dyad is (10^00) and (02^00). The notation $(10^00)_I$ and $(10^00)_{II}$ is used in Ref. 23 for the same levels.) As shown in Table 1, in the range between 2306 and 2308 cm^{-1}, at least one transition is accessible for each of the levels excited by the discharge. The intensity of absorption of the diode laser intensity for any absorption line $(v_1v_2^lv_3)\rightarrow(v_1v_2^lv_3+1)$ of CO_2 is related to $N_{v_1v_2^lv_3}$, the density of molecules in state $v_1v_2^lv_3$, via the equation,

Table 1. CO_2 vibrational transitions near 2307 cm^{-1}.

line	Transition	Freq. (cm^{-1})	S_{300}	S_{400}
1	$00^00\rightarrow00^01$ P_{46}	2306.927	0.00299	0.00617
2	$00^01\rightarrow00^02$ P_{21}	2306.636	0.0662	0.0617
3	$00^02\rightarrow00^03$ R_{10}	2307.296	0.101	0.0796
4	$01^10\rightarrow01^11_f$ P_{34}	2306.611	0.0137	0.0179
5	$01^10\rightarrow01^11_e$ P_{33}	2307.653	0.0151	0.0191
6	$01^11\rightarrow01^12_f$ P_7	2307.758	0.0340	0.0259
7	$01^11\rightarrow01^12_e$ P_6	2306.959	0.0404	0.0310
8	$02^20\rightarrow02^21_f$ P_{21}	2306.424	0.0328	0.0306
9	$02^20\rightarrow02^21_e$ P_{20}	2307.327	0.0338	0.0309
10	$02^21\rightarrow02^22_f$ R_{10}	2307.390	0.0649	0.0513
11	$02^21\rightarrow02^22_e$ R_9	2306.679	0.0608	0.0476
12	$03^30\rightarrow03^31$ P_6	2306.870	0.0156	0.0119
13	$10^00\rightarrow10^01$ P_{24}	2306.150	0.0292	0.0290
14	$10^01\rightarrow10^02$ R_5	2306.422	0.0425	0.0324
15	$02^00\rightarrow02^01_f$ P_{24}	2307.054	0.0292	0.0290
16	$02^01\rightarrow02^02_f$ R_5	2306.897	0.0213	0.0162

$$\ln\frac{I}{I_0} = \frac{-8\pi^3 \nu N_{v_1 v_2^l v_3}}{3hc} |R_{00^0 1 - 00^0 0}|^2 S_T \Delta x.$$

Where S_T is defined by,

$$S_T = \frac{(m^2 - l^2)}{|m|} e^{\frac{-B''J''(J''+1)hc}{kT}}.$$

The quantity S_T is the relative strength factor at the temperature T. S_T relates the line strength of a given ro-vibrational transition to the density of molecules in a given vibrational state. We have calculated this quantity for 300 and 400 K and have listed these values for the transitions in Table 1.

Experiments were performed to determine the distributions of states formed. For the first set of experiments, a flow of room temperature CO_2 was monitored as it flowed passed the first observation port (see Figure 9). Five separated lines were recorded in the region between 2306.9 and 2307.7 cm^{-1}. These lines along with their spectroscopic assignments, are shown in Table 2.

Table 2. Assignments of spectroscopic lines near 2307 cm^{-1}.

Spectroscopic Assignment	-ln(I/Io)	Relative density (measured)	Relative density (Boltzmann)
0000→0001	0.72	1	1
Mixture of four isotopic lines	0.117		
$02^20 \rightarrow 02^21$	0.037	0.0045	0.0049
$C^{12}O^{18}O^{16}$	0.025		
$01^10 \rightarrow 01^11$	0.34		

The signal strengths of the lines attributable to $C^{12}O_2{}^{16}$ were converted to densities relative to the ground state density using the values of S_{300} in Table 1. These are also reported in Table 2 along with the values calculated for a Boltzmann distribution at 300K. As shown, the measured densities are in good agreement with the Boltzmann distribution. This indicates that our spectroscopic assignments are indeed correct and confirms that

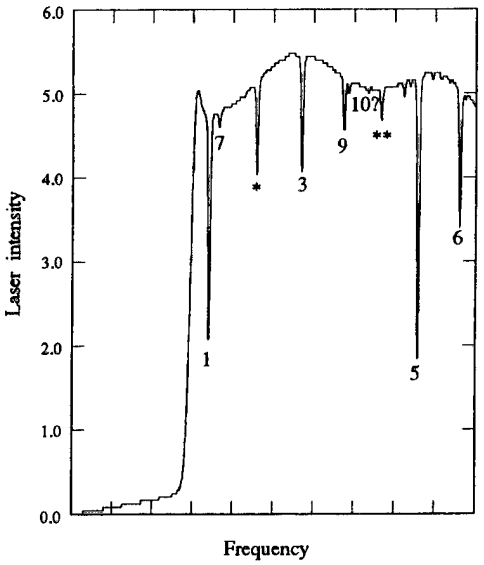

Figure 11. Spectrum of discharged CO_2 near 2307 cm^{-1}. Assignment numbers are those of Table 1. * Composition of four lines of different isotopes. ** $C^{12}O^{18}O^{16}$ line.

we can make quantitative density measurements to determine the vibrational population of CO_2.

In a second experiment, CO_2 was excited by passing it through a microwave discharge. Figure 11 shows the spectrum of states near 2307 cm^{-1} that we observed at the first observation point under these conditions. The major features of the spectrum were assigned using Table 1. The intensities of the lines and their calculated relative densities at 400K are shown in Table 3.

As shown, the only states excited significantly at the first observation point are the 01^10 and the 01^11 states. Additional data taken at the second and subsequent observation points shows that the 01^10 state is the only state to be significantly populated above its equilibrium value. This experiment confirms the results of Bailly and coworkers for discharge flows of CO_2.[26]

Under our experimental conditions then, when a microwave discharge is applied to a flow of CO_2, the CO_2 is excited to a number of vibrational modes. These modes, however, are quickly quenched and relax to a distribution which is dominated by the 01^10 state. We estimate that equation (14) can be used to analyze the deactivation of the 01^10 state with an incurred error of less than 20%.

Table 3. Intensities and calculated densities of assigned lines in discharged CO_2.

Assignment (see Table 1)	Intensity	Relative density (400K)
1	0.842	1.
7	0.040	0.009
15	0.241	0.06
3	0.289	0.03
9	0.121	0.03
10	<0.01	<0.001
5	1.034	0.40
6	0.393	0.11

4.3.2 Preliminary Experiments to Measure CO_2 Deactivation by Atomic Oxygen. Experiments were performed to measure the deactivation of CO_2 (01^10) by atomic oxygen. A mixed stream containing vibrationally-excited CO_2 and O_2 was prepared as described above (Section 4.2). The absorption signal for the $01^10 \rightarrow 00^00$ transition in CO_2 was monitored at all four observation ports.

The procedure used for reducing these data follows: The CO_2 discharge was turned on and measurements were taken at each of the four ports in the flow reactor. These measurements provided the data for what we shall refer to as the deactivation series. A second series of measurements was taken with the CO_2 discharge off. The second series provided the equilibrium concentrations of CO_2 at each of the four ports. The values of the equilibrium concentrations of CO_2 were subtracted from the values obtained in the deactivation set and the logarithm of the difference was plotted as a function of reaction time (distance down the flow reactor).

Two more series of measurements (one deactivation and one equilibrium series) were taken after the addition of the atomic oxygen. As above, the first set was with the CO_2 discharge turned on and the second set with the discharge off. These sets were also plotted logarithmically as a function of reaction time in a manner similar to that described for the first two sets. The difference in the slopes of the two curves was taken to represent the deactivation by atomic oxygen.

Typical deactivation data using this procedure is shown in Figure 12. Reduction of the data such as that shown indicated the deactivation of CO_2 (01^10) to be $\sim 10^{-14}$ cm^3 molecule^{-1}s^{-1}. This result was in conflict with the fast rate attributed to this reaction.

A problem with our experimental procedure was subsequently uncovered which put our result

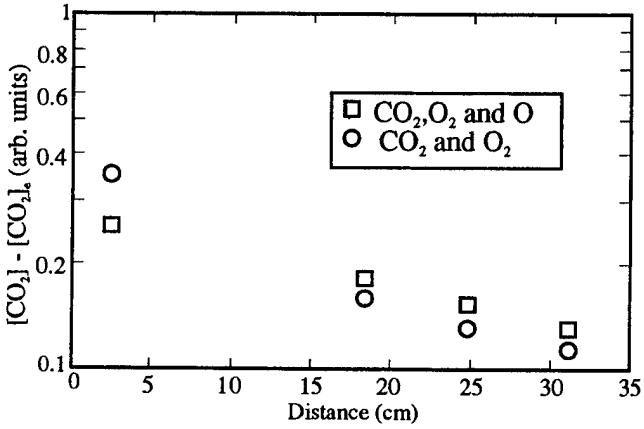

Figure 12. Preliminary experiments to determine the deactivation of $CO_2(01^10)$ by O.

in doubt. During the course of these experiments a subtle effect was noted in the temperature of the flowing gas stream. When the microwave discharge was initially turned on, the temperature of the gas stream rose about 15° above ambient. This effect was anticipated and is due to the heating of the CO_2 from v-t energy transfer. What was not anticipated was a slow but steady increase in the temperature of the gas stream as a function of time. At 20 minutes after the discharge was turned on, the temperature of the gas stream measured near the third observation port increased another 30°C. The transit time of the gas through the reactor is of the order of tens of milliseconds. Therefore it was not expected that the gas temperature would continue to increase tens of minutes after the discharge was turned on.

The explanation of this effect is that the major deactivation of the vibrationally-excited gas oc-

curs by wall collisions. The wall collisions gradually heated the flow reactor while the hot walls of the reactor, in turn, heated the flowing gas.

This affected our results in the following manner: Averaging of the spectra at each of the four observation ports took about 30-40 minutes. As a result of this long averaging time, the equilibrium series (the series with the CO_2 discharge off), was taken at a temperature which was considerably colder than the temperature of the deactivation series. The equilibrium concentration of CO_2 is a steep function of temperature, therefore this procedure induced a large error in the concentration measurements. Since the temperature was higher for the deactivation series than the equilibrium series, the net result was to make the CO_2 concentrations appear to be anonymously high and make the deactivation appear slower than it actually was.

4.3.3 Measurement of the Deactivation of $CO_2(01^10)$ by Helium and Argon and Oxygen. A new procedure was adopted to take account of the affect of this slow heating. In this procedure, the deactivation series and equilibrium series CO_2 concentrations were obtained at each of the observation points by alternately measuring the CO_2 concentration with the discharge on and with the discharge off. This alternating procedure was repeated nine times at each observation port for each series. Under these circumstances the temperature variation was held to within 5°C at each observation port.

4.3.3.1 Preliminary Experiments. A preliminary set of experiments were performed to obtain an order of magnitude comparison of the rates of deactivation of $CO_2(01^10)$ by He, Ar and O. For these experiments, the $CO_2(01^10)$ concentration was monitored at the second observation port. The decrease of $CO_2(01^10)$ after the addition of approximately equal flows of He, Ar and O is shown in Table 4.

Table 4. Results of preliminary deactivation experiments using new procedure.

Species	$[CO_2(01^10)]$ decrease (arbitray units)
He	24±2
Ar	2±2
O	30±2

The rate of deactivation of $CO_2(01^10)$ is known to be approximately three orders of magnitude greater than the deactivation by Ar. [27,28] As shown in Table 4, under these conditions the deactivation by He is much faster than that obtained by Ar. The value obtained for Ar is not significantly greater than zero. This result is in agreement with the aforementioned fact that He is a much faster deactivator of $CO_2(01^10)$ than Ar. Of significance here is the fact that the deactivation of CO_2 by atomic oxygen is shown to be at least as fast as deactivation of CO_2 by He.

4.3.3.2 Measurement of the Deactivation of $CO_2(01^10)$ by Helium and Argon. These experiments were performed by obtaining a deactivation and an equilibrium series before and after the addition of the deactivating species. Each series consisted of nine determinations of the CO_2 concentration using the new procedure as described in Section 4.3.3. Each of the deactivation experiments (CO_2 alone,CO_2+He, and CO_2+Ar was performed twice on separate days. The species concentration for these experiments are shown in Table 5.

Table 5. Species concentrations for the experiments to determine the deactivation of $CO_2(01^10)$ by He and Ar.

Species	Partial pressure (Torr)
CO_2	0.33
He	0.050
Ar	0.065

The results of these experiments were averaged and are shown in Figure 13. These experiments yield a value of $1.5\pm0.5\times10^{-13}$ $cm^3molecule^{-1}s^{-1}$ for the deactivation of $CO_2(01^10)$ by He at 290K. Under our experimental conditions the deactivation by Ar is not measurable at 297K.

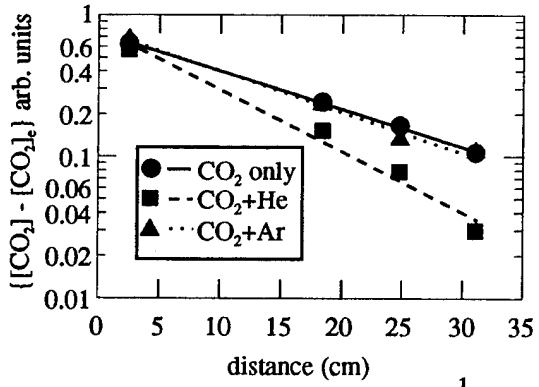

Figure 13. The deactivation of $CO_2(01^10)$ by He and Ar.

As shown in equation (13), the slope of the plots in Figure 13 represent the sum of the rates for the forward and backward steps in reaction (12). Near 300 K the ratio of the (01^10) concentration to the concentration of the (00^00) state is 0.04. Therefore we conclude the rate for deactivation of $CO_2(01^10)$ by He is $1.4\pm0.5\times10^{-13}$ $cm^3molecule^{-1}s^{-1}$ while the rate for the reverse reaction is $4\pm1\times10^{-13}$ $cm^3molecule^{-1}s^{-1}$. This result is in good agreement with the results of Wickham-Jones et. al.[28] who measured a rate of $1.0\pm0.1\times10^{-13}$ $cm^3molecule^{-1}s^{-1}$ for the deactivation by helium at 295K.

Lunt et. al.[27] have measured the deactivation by argon at 295K to be $5.9\pm7.4\%\times10^{-16}$ $cm^3molecule^{-1}s^{-1}$. This slow rate would preclude its measurement under our experimental conditions, again in agreement with our results.

4.3.3.3 Measurement of the Deactivation of $CO_2(01^10)$ by Atomic Oxygen. These experiments were performed in a manner similar to those described in Section 4.3.3.2. Each series consisted of nine determinations of the CO_2 concentration using the new procedure as described in Section 4.3.3. Each of the deactivation experiments (CO_2 alone, CO_2+O_2 and CO_2+O_2+O) was performed twice on separate days. The atomic oxygen was formed by passing the O_2 through a microwave discharge. The species concentration for these experiments are shown in Table 6.

Table 6. Species concentrations for the experiments to determine the deactivation of $CO_2(01^10)$ by O.

Species	Partial pressure (Torr)
CO_2	0.33
O_2	0.13
O	0.014

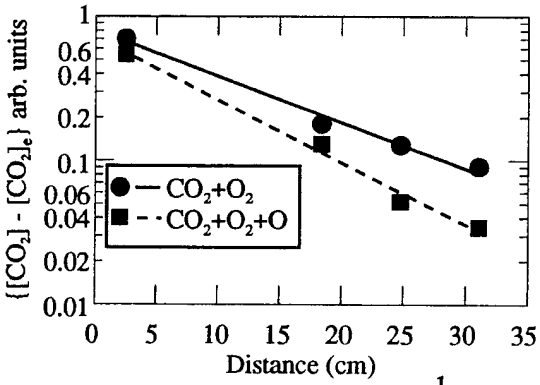

Figure 14. The deactivation of $CO_2(01^10)$ by O.

The results of these experiments were averaged and are shown in Figure 14.

These experiments yielded a rate for deactivation by O of $5\pm2\times10^{-13}$ $cm^3molecule^{-1}s^{-1}$ at 301K. Using the procedure described in Section 4.3.3.2, we concluded the rate for the deactivation of $CO_2(01^10)$ by O at 301K is $5\pm2\times10^{-13}$ $cm^3molecule^{-1}s^{-1}$, while the rate for the back reaction is $2\pm0.8\times10^{-13}$ $cm^3molecule^{-1}s^{-1}$. This result is in reasonable agreement with the estimate of Shved[22] et al. of $\sim1\times10^{-12}$ $cm^3molecule^{-1}s^{-1}$ from their experiment, while it is in excellent agreement with the value used by Sharma and coworkers[1] to model the upper atmosphere.

5. Conclusions.

The deactivation of NO(v=1) by atomic oxygen has a rate constant of $5\pm1\times10^{-11}$ $cm^3molecule^{-1}s^{-1}$ from 200-350K. By including the work of Glanzer and Troe, this range can be extended to 2700K. The deactivation is fast (~10 gas kinetic collisions) and has little temperature dependence. These observations are consistent with a model where the deactivation occurs via an NO_2* complex. The reaction may occur via a collision between O and NO which creates an electronically-excited NO_2 molecule followed by a curve-crossing mechanism where NO_2 dissociates into O and NO in their vibrational ground states. The large rate constant for NO deactivation by NO_2 may be attributable to a similar mechanism involving an N_2O_3 complex.

The deactivation of $CO_2(01^10)$ by atomic oxygen has a rate constant of $5\pm2\times10^{-13}$ $cm^3molecule^{-1}s^{-1}$ at 301K. This result is similar to the result for deactivation of NO(v=1) by atomic oxygen in that the rate for deactivation is anomalously fast in comparison with other deactivators of comparable size and mass. This result may be indicative of a mechanism involving a CO_3 complex.

6. References

1. Sharma R. D. and Nadile R. M., "Carbon Dioxide ν_2 Radiance Results Using a New Non-Equilibrium Model," Paper No. AIAA-81-0426 AIAA 19th Aerospace Sciences Meeting, 12-15 Jan. 1987, St. Louis, MO.

2. Sharma R. D. and Wintersteiner P. P., "CO_2 Component of Daytime Earth Limb Emission at 2.7 μm," J. Geophys. Res. **90,** A10, 9789-9803 (1985).

3. Calodonia G. E., Green B. D. and Nadile R. M., "The Analysis of SPIRE Measurements of Atmospheric Limb CO_2 ν_2 Fluorescence," J. Geophys. Res. **90,** A10, 9783-9788 (1985).

4. Stair A. T., Jr., Sharma R. D., Nadile R. M., Baker D. J. and Grieder W. F., "Observations of Limb Radiance With Cryogenic Spectral Infrared Rocket Experiment," J. Geophys. Res. **90**, A10, 9763-9775 (1985).

5. Zachor A. S., Sharma R. D., Nadile R. M. and Stair A. T., Jr., "Inversion of a Spectrally Resolved Limb Radiance Profile for the NO Fundamental Band," J. Geophys. Res. **90,** A10, 9776-9782 (1985).

6. Kockarts G., "Nitric Oxide Cooling in the Terrestrial Thermosphere," Geophys. Res. Letters, **7**, 137-140 (1980).

7. Fernando R. and Smith I., "Vibrational Relaxation of NO by Atomic Oxygen," Chem. Phys. Lett., **66**, 218-222 (1979).

8. Glazer K. and Troe J., "Vibrational Relaxation of NO in Collisions with Atomic Oxygen and Chlorine," J. Chem. Phys. **63**, 4352-4357, (1975).

9. Stephenson J. C. and Freund S. M.,"Infrared Laser Enhanced Reactions: Chemistry of NO(v=1) with O_3," J. Chem. Phys. **65**, 1893-1900 (1975).

10. Amiot C. J., "Spectral Coincidences Between CO Laser Lines and Absorption Lines of NO," Phys. B Atomic and Molec. Phys. **10**, L317-320 (1977).

11. Bradburn G. R. and Lilenfeld H. V., "Absolute Emission Rate of the Reaction Between Nitric Oxide and Atomic Oxygen," J. Phys. Chem. **92**, 5266-5270 (1988).

12. Westenberg A. A., "Use of ESR for the Quantitative Determination of Gas Phase Atom and Radical Concentrations," in Progress in Reaction Kinetics, Jenning K. R. and Cundall R. B., eds., Pergamon Press Vol 7., Part 1, 23-82 (1973).

13. Westenberg A. A. and deHaas N., "Quantitative Measurements of Gas Phase O and N Atom Concentrations by ESR," J. Chem. Phys. **40**, 3087-3098 (1964).

14. Lilenfeld H.V. and Richardson R. J., " The ESR Spectrum and Linewidth Measurements of Atomic Iodine," J. Chem. Phys. **70**, 3859-3862 (1974).

15. Lilenfeld H. V., Carr P. A. G. and Hovis F. E., "Energy Pooling Reactions in the Oxygen-Iodine System," J. Chem. Phys. **81**, 5730-5736 (1984).

16. Kaufman F., "Reactions of Oxygen Atoms," in Progress in Reaction Kinetics, Porter G., ed., Vol. 1, 1-40 (1961).

17. Farrow L. A. and Richton R., "Extinction Coefficient of the $R_{1/2}$ (25/2) NO Transition at the 8-7 P(11) CO," Applied Optics **18**, 597-599 (1979).

18. More J. J., Garbow B. S. and Hillstrom K. E., "User Guide for MINPACK-1," Argonne National Laboratory Report ANL-80-74 (1980).

19. Greene B. D., Caledonia G. E., Murphy R. E. and Robert F. X., "The Vibrational Relaxation of NO(v=1-7) by O_2," J. Chem. Phys. **76**, 2441-2448 (1982).

20. Stephenson J. C., "Vibrational Relaxation of NO $X\ ^2\pi$(v=1) in the Temperature Range 100-300K," J. Chem. Phys. **60**, 4289-4294 (1974).

21. Center R. E., "Vibrational Relaxation of CO_2 by O Atoms," J. Chem. Phys. **59**, 3523-3527 (1973).

22. Shved G. M., Khvorostovskaya L. E., Potekhin I. Y., Yanikov A. I., Kutepov A. A.

and Fomichev, V. I., "Measurement of the Quenching Rate Constant of $CO_2(0,11,0)$-O Collisions and Its Significance for the Thermal Regime and Radiation in the Lower Thermosphere," Izvestiya, Atmos. and Oceanic Physics **27**, 295-299 (1991).

23. Bailly D., Farrenq R., Guelachvilli G. and Rossetti C., "$^{12}C^{16}O_2$ Analysis of Emission Fourier Spectra in the 4.5 μ Region: Rovibrational Transitions $0v_2^1v_3$-$0v_2^1(v_3-1)$, $v_2 = 1$," Journal of Molec. Spectros. **90**, 74-105 (1981).

24. Bailly D. and Rossetti C., "$^{12}C^{16}O_2$ Spectroscopic Constants of the Fermi Dyad [10^0v_3, 02^0v_3] and Wavenumbers of Laser Sequence Band Transitions," Optics Commun. **42**, 323-328 (1982).

25. Guelachvelli G. and Rao K. N., Handbook of Infrared Standards with Spectral Maps and Transition Assignments between 3 and 2600 mm, Academic Press (1986).

26. Bailly D., Rossetti C. and Guelachvili G., "$^{12}C^{16}O_2$: Vibrational Population Distributions in CO_2-N_2, CO_2-He and CO_2-N_2-He DC Discharges from High Information Emission Fourier Spectra," Chem. Phys. **100**, 101-118 (1985).

27. Lunt S. L., Wickham-Jones C. T. and Simpson C. J. S. M., "Rate Constants for the Deactivation of the 15 μm Band of Carbon Dioxide by the Collision Partners CH_3F, CO_2, N_2, Ar, and Kr," Chem. Phys. Lett. **115**, 60-64 (1985).

28. Wickham-Jones C. T. and Simpson C. J. S. M., "Experimental and Theoretical Determination of the Rate Constants for Vibrational Relaxation of CO_2 and CH_3F by He," Chem. Phys. **117**, 9, 9-16 (1987).

7. Appendix

The results of our calculations for the energies of the $(v_1v_2^lv_3)\rightarrow(v_1v_2^lv_3+1)$ transitions in CO_2 follow.

v"-v'	0000-0001	0000-0001	0001-0002	0001-0002
J	P	R	P	R
0	2350.143	2349.918		
1			2323.409	2325.713
2	2347.576	2351.448		
3			2321.842	2327.219
4	2345.985	2352.953		
5			2320.250	2328.700
6	2344.368	2354.434		
7			2318.634	2330.156
8	2342.728	2355.890		
9			2316.994	2331.587
10	2341.062	2357.321		
11			2315.328	2332.994
12	2339.373	2358.728		
13			2313.639	2334.376
14	2337.659	2360.109		
15			2311.925	2335.733
16	2335.920	2361.466		
17			2310.186	2337.065
18	2334.157	2362.799		
19			2308.424	2338.373
20	2332.369	2364.106		
21			2306.636	2339.656
22	2330.558	2365.388		
23			2304.825	2340.913
24	2328.722	2366.646		
25			2302.989	2342.146
26	2326.861	2367.878		
27			2301.129	2343.354
28	2324.976	2369.086		
29			2299.245	2344.537
30	2323.068	2370.269		
31			2297.336	2345.695
32	2321.134	2371.426		
33			2295.403	2346.828
34	2319.177	2372.559		
35			2293.446	2347.936
36	2317.196	2373.667		
37			2291.465	2349.019
38	2315.190	2374.749		
39			2289.460	2350.077
40	2313.161	2375.807		
41			2287.431	2351.110
42	2311.107	2376.839		
43			2285.377	2352.117
44	2309.029	2377.847		

v"-v'	0002-0003	0002-0003	0110f-0111f	0110f-0111f
J	P	R	P	R
0				
1				
2	2297.710	2301.520	2335.062	2338.944
3				
4	2296.143	2303.001	2333.466	2340.453
5				
6	2294.552	2304.457	2331.846	2341.939
7				
8	2292.936	2305.889	2330.202	2343.399
9				
10	2291.295	2307.296	2328.533	2344.835
11				
12	2289.630	2308.678	2326.839	2346.247
13				
14	2287.941	2310.035	2325.122	2347.633
15				
16	2286.227	2311.368	2323.380	2348.995
17				
18	2284.489	2312.676	2321.613	2350.332
19				
20	2282.726	2313.959	2319.823	2351.645
21				
22	2280.940	2315.217	2318.008	2352.933
23				
24	2279.128	2316.450	2316.169	2354.195
25				
26	2277.293	2317.659	2314.306	2355.433
27				
28	2275.433	2318.842	2312.418	2356.647
29				
30	2273.550	2320.001	2310.507	2357.835
31				
32	2271.642	2321.134	2308.571	2358.998
33				
34	2269.709	2322.243	2306.611	2360.137
35				
36	2267.753	2323.327	2304.627	2361.250
37				
38	2265.773	2324.385	2302.620	2362.339
39				
40	2263.768	2325.419	2300.588	2363.402
41				
42	2261.740	2326.427	2298.532	2364.441
43				
44	2259.687	2327.411	2296.452	2365.454

v''-v'	0110e-0111e	0110e-0111e	0111f-0112f	0111f-0112f
J	P	R	P	R
0				
1			2310.925	2313.236
2				
3	2334.271	2339.697	2309.354	2314.746
4				
5	2332.666	2341.193	2307.758	2316.231
6				
7	2331.036	2342.664	2306.138	2317.692
8				
9	2329.382	2344.110	2304.494	2319.128
10				
11	2327.704	2345.532	2302.825	2320.539
12				
13	2326.002	2346.930	2301.132	2321.926
14				
15	2324.276	2348.303	2299.415	2323.289
16				
17	2322.525	2349.651	2297.673	2324.626
18				
19	2320.750	2350.975	2295.907	2325.939
20				
21	2318.952	2352.274	2294.117	2327.227
22				
23	2317.129	2353.548	2292.302	2328.490
24				
25	2315.282	2354.798	2290.463	2329.729
26				
27	2313.411	2356.023	2288.601	2330.942
28				
29	2311.516	2357.224	2286.714	2332.131
30				
31	2309.597	2358.400	2284.803	2333.295
32				
33	2307.654	2359.550	2282.868	2334.434
34				
35	2305.687	2360.677	2280.908	2335.548
36				
37	2303.696	2361.778	2278.925	2336.637
38				
39	2301.681	2362.855	2276.918	2337.701
40				
41	2299.643	2363.906	2274.887	2338.741
42				
43	2297.581	2364.933	2272.832	2339.755
44				

v''-v'	0111e-0112e	0111e-0112e	0220f-0221f	0220f-0221f
J	P	R	P	R
0				
1			2323.358	2325.690
2	2310.145	2313.990		
3			2321.773	2327.214
4	2308.564	2315.486		
5			2320.164	2328.714
6	2306.959	2316.957		
7			2318.531	2330.189
8	2305.330	2318.404		
9			2316.873	2331.641
10	2303.676	2319.826		
11			2315.192	2333.067
12	2301.998	2321.223		
13			2313.486	2334.470
14	2300.296	2322.597		
15			2311.757	2335.848
16	2298.570	2323.945		
17			2310.003	2337.202
18	2296.820	2325.269		
19			2308.225	2338.531
20	2295.045	2326.569		
21			2306.424	2339.835
22	2293.246	2327.843		
23			2304.598	2341.115
24	2291.424	2329.094		
25			2302.748	2342.371
26	2289.577	2330.319		
27			2300.875	2343.602
28	2287.706	2331.520		
29			2298.977	2344.808
30	2285.812	2332.696		
31			2297.056	2345.990
32	2283.893	2333.847		
33			2295.111	2347.147
34	2281.951	2334.974		
35			2293.143	2348.280
36	2279.984	2336.076		
37			2291.150	2349.387
38	2277.994	2337.153		
39			2289.134	2350.471
40	2275.980	2338.205		
41			2287.094	2351.529
42	2273.942	2339.232		
43			2285.031	2352.562
44	2271.880	2340.235		

v''-v'	0220e-0221e	0220e-0221e	0221f-0222f	0221f-0222f
J	P	R	P	R
0				
1				
2	2322.568	2326.455	2297.680	2301.536
3				
4	2320.972	2327.967	2296.095	2303.036
5				
6	2319.350	2329.455	2294.486	2304.511
7				
8	2317.705	2330.918	2292.853	2305.963
9				
10	2316.036	2332.357	2291.196	2307.390
11				
12	2314.342	2333.772	2289.514	2308.792
13				
14	2312.624	2335.162	2287.809	2310.171
15				
16	2310.883	2336.528	2286.079	2311.524
17				
18	2309.117	2337.869	2284.326	2312.854
19				
20	2307.327	2339.186	2282.548	2314.159
21				
22	2305.514	2340.479	2280.747	2315.439
23				
24	2303.676	2341.747	2278.921	2316.695
25				
26	2301.815	2342.990	2277.072	2317.926
27				
28	2299.930	2344.209	2275.199	2319.133
29				
30	2298.021	2345.403	2273.302	2320.315
31				
32	2296.088	2346.573	2271.381	2321.472
33				
34	2294.131	2347.718	2269.437	2322.605
35				
36	2292.151	2348.838	2267.468	2323.713
37				
38	2290.147	2349.934	2265.476	2324.797
39				
40	2288.119	2351.005	2263.460	2325.856
41				
42	2286.068	2352.052	2261.421	2326.890
43				
44	2283.993	2353.074	2259.358	2327.899

v''-v'	0221e-0222e	0221e-0222e	0330-0331	0330-0331
J	P	R	P	R
0				
1	2298.463	2300.777	2310.883	2313.220
2			2310.093	2313.986
3	2296.890	2302.289	2309.296	2314.747
4			2308.493	2315.502
5	2295.293	2303.777	2307.684	2316.250
6			2306.870	2316.993
7	2293.672	2305.240	2306.049	2317.730
8			2305.222	2318.460
9	2292.027	2306.679	2304.390	2319.185
10			2303.551	2319.903
11	2290.358	2308.094	2302.706	2320.616
12			2301.856	2321.322
13	2288.664	2309.485	2300.999	2322.023
14			2300.137	2322.717
15	2286.947	2310.851	2299.268	2323.405
16			2298.394	2324.088
17	2285.206	2312.192	2297.514	2324.764
18			2296.627	2325.434
19	2283.440	2313.509	2295.735	2326.098
20			2294.837	2326.756
21	2281.651	2314.802	2293.933	2327.408
22			2293.023	2328.054
23	2279.837	2316.070	2292.107	2328.694
24			2291.185	2329.328
25	2278.000	2317.314	2290.257	2329.955
26			2289.324	2330.577
27	2276.139	2318.533	2288.384	2331.192
28			2287.438	2331.802
29	2274.254	2319.728	2286.487	2332.405
30			2285.530	2333.002
31	2272.345	2320.898	2284.567	2333.593
32			2283.598	2334.178
33	2270.413	2322.043	2282.623	2334.757
34			2281.642	2335.330
35	2268.456	2323.164	2280.655	2335.897
36			2279.663	2336.457
37	2266.476	2324.260	2278.664	2337.012
38			2277.660	2337.560
39	2264.473	2325.332	2276.650	2338.103
40			2275.634	2338.639
41	2262.445	2326.379	2274.612	2339.169
42			2273.584	2339.693
43	2260.395	2327.401	2272.551	2340.211
44			2271.511	2340.722

v''-v'	0221e-0222e	0221e-0222e	0330-0331	0330-0331
J	P	R	P	R
0				
1	2298.463	2300.777	2310.883	2313.220
2			2310.093	2313.986
3	2296.890	2302.289	2309.296	2314.747
4			2308.493	2315.502
5	2295.293	2303.777	2307.684	2316.250
6			2306.870	2316.993
7	2293.672	2305.240	2306.049	2317.730
8			2305.222	2318.460
9	2292.027	2306.679	2304.390	2319.185
10			2303.551	2319.903
11	2290.358	2308.094	2302.706	2320.616
12			2301.856	2321.322
13	2288.664	2309.485	2300.999	2322.023
14			2300.137	2322.717
15	2286.947	2310.851	2299.268	2323.405
16			2298.394	2324.088
17	2285.206	2312.192	2297.514	2324.764
18			2296.627	2325.434
19	2283.440	2313.509	2295.735	2326.098
20			2294.837	2326.756
21	2281.651	2314.802	2293.933	2327.408
22			2293.023	2328.054
23	2279.837	2316.070	2292.107	2328.694
24			2291.185	2329.328
25	2278.000	2317.314	2290.257	2329.955
26			2289.324	2330.577
27	2276.139	2318.533	2288.384	2331.192
28			2287.438	2331.802
29	2274.254	2319.728	2286.487	2332.405
30			2285.530	2333.002
31	2272.345	2320.898	2284.567	2333.593
32			2283.598	2334.178
33	2270.413	2322.043	2282.623	2334.757
34			2281.642	2335.330
35	2268.456	2323.164	2280.655	2335.897
36			2279.663	2336.457
37	2266.476	2324.260	2278.664	2337.012
38			2277.660	2337.560
39	2264.473	2325.332	2276.650	2338.103
40			2275.634	2338.639
41	2262.445	2326.379	2274.612	2339.169
42			2273.584	2339.693
43	2260.395	2327.401	2272.551	2340.211
44			2271.511	2340.722

v''-v'	1000-1001	1000-1001	1001-1002	1001-1002
J	P	R	P	R
0	0000.000	2327.372		
1			2301.135	2303.438
2	2325.031	2328.902		
3			2299.568	2304.943
4	2323.439	2330.406		
5			2297.976	2306.422
6	2321.822	2331.886		
7			2296.359	2307.876
8	2320.180	2333.340		
9			2294.717	2309.305
10	2318.514	2334.769		
11			2293.050	2310.709
12	2316.822	2336.173		
13			2291.358	2312.088
14	2315.105	2337.552		
15			2289.641	2313.442
16	2313.364	2338.906		
17			2287.900	2314.771
18	2311.598	2340.235		
19			2286.134	2316.074
20	2309.807	2341.538		
21			2284.343	2317.352
22	2307.991	2342.816		
23			2282.527	2318.605
24	2306.150	2344.069		
25			2280.686	2319.832
26	2304.285	2345.297		
27			2278.821	2321.035
28	2302.395	2346.499		
29			2276.930	2322.211
30	2300.480	2347.676		
31			2275.016	2323.363
32	2298.541	2348.828		
33			2273.076	2324.489
34	2296.577	2349.954		
35			2271.112	2325.590
36	2294.589	2351.055		
37			2269.123	2326.666
38	2292.576	2352.131		
39			2267.110	2327.716
40	2290.538	2353.181		
41			2265.072	2328.741
42	2288.476	2354.206		
43			2263.010	2329.740
44	2286.389	2355.206		

v''-v'	0200-0201	0200-0201	0201-0202	0201-0202
J	P	R	P	R
0	2528.433	2328.208		
1			2301.597	2303.904
2	2325.865	2329.740		
3			2300.029	2305.412
4	2324.273	2331.248		
5			2298.437	2306.897
6	2322.658	2332.733		
7			2296.822	2308.358
8	2321.019	2334.193		
9			2295.183	2309.794
10	2319.356	2335.630		
11			2293.521	2311.207
12	2317.669	2337.042		
13			2291.834	2312.596
14	2315.959	2338.430		
15			2290.124	2313.961
16	2314.225	2339.795		
17			2288.391	2315.301
18	2312.468	2341.135		
19			2286.634	2316.618
20	2310.687	2342.451		
21			2284.854	2317.911
22	2308.882	2343.743		
23			2283.050	2319.179
24	2307.054	2345.011		
25			2281.222	2320.423
26	2305.202	2346.254		
27			2279.371	2321.643
28	2303.327	2347.473		
29			2277.497	2322.839
30	2301.429	2348.668		
31			2275.600	2324.011
32	2299.507	2349.839		
33			2273.679	2325.158
34	2297.562	2350.985		
35			2271.734	2326.281
36	2295.593	2352.107		
37			2269.767	2327.380
38	2293.601	2353.205		
39			2267.776	2328.454
40	2291.586	2354.278		
41			2265.762	2329.504
42	2289.548	2355.326		
43			2263.725	2330.529
44	2287.486	2356.350		